Supporting Information

Ligand Field Effects and the High Spin-High Reactivity Correlation in the H Abstraction by Non-Heme Iron(IV)-Oxo Complexes: A DFT Frontier Orbital Perspective

Andranik Kazaryan and Evert Jan Baerends[*]

VU University Amsterdam, Theoretical Chemistry, FEW, De Boelelaan 1083, 1081 HV Amsterdam, The Netherlands

E-mail: a.k.kazaryan@gmail.com,E.J.Baerends@vu.nl

---

[*]To whom correspondence should be addressed

According to the analysis discussed in the main text, the reactivities of the considered compounds order in a sequence: $^5\mathbf{1} > {}^3\mathbf{1} \approx {}^5\mathbf{2} > {}^3\mathbf{2}$. In order to investigate the energy contributions, an energy decomposition analysis has been carried out. To this end we used the scheme,[1] implemented in ADF,[2–4] in which the total bonding energy is given by

$$\Delta E = \Delta E^{Strain} + \Delta E^{Pauli} + \Delta E^{Elstat} + \Delta E^{Orb}, \tag{1}$$

where ΔE^{Pauli}, ΔE^{Elstat} and ΔE^{Orb} are the Pauli repulsion, electrostatic and orbital attraction components. ΔE^{Strain} is the deformation energy required to bring the reactants together to form a complex. To determine the strain energy, we calculated the energies of the reactants (oxidant and methane) in their distorted geometries corresponding to the structures along the intrinsic reaction coordinate (IRC). The energies of the distorted structures relative to the free reactant energies represent the strain contributions.

For the decomposition of electronic energy we used the fragment analysis where the system has been separated into two fragments: the oxidant and the substrate. The orbitals that are used in the analysis come from spin-restricted calculations on the fragments. This has little effect on e.g. the orbital populations, since the orbitals do not change significantly by spin polarization (and the populations are a qualitative measure anyway). As for the energy decomposition, this is not done with spin-restricted densities, but the ADF allows to use as the reference fragment densities fully spin-polarized densities that arise from spin-unrestricted population (different α and β populations) of the restricted orbitals. This is the largest effect of the open-shell nature of the fragments, only the effect of further change in the orbitals if fully self-consistent calculations with different orbitals for different spin would be done is neglected here.

The total bonding energy is divided into the strain and the electronic energy. The strain contributions along the reaction path (projected on the C-H coordinate for clarity) are shown in Figures S1-S2. The electronic energy is composed of the Pauli repulsion, electrostatic and orbital attraction.

The full decomposition of the transition state energy is listed in Table S1.

It is seen from the table that in the triplet state ^{3}**1** compound the main contribution is from the strain of the oxidant, whereas the methane strain is smaller than in the respective quintet system. The latter is due to an earlier transition state: CH=1.316Å (see Table S2). A weaker Pauli repulsion is compensated by a smaller orbital and electrostatic attraction.

When comparing systems ^{5}**1** and ^{5}**2**, it is apparent that the net rise of the barrier is due to the total strain which outweighs the stronger electronic attraction in ^{5}**2**. The stronger electronic interaction originates from the shorter OH distance: 1.124 Å versus 1.206 Å in ^{5}**1**.

A spin change in compound **2** from quintet to triplet leads to a ca. 15 kcal/mol higher barrier which is a steric effect mainly due to the much stronger Pauli repulsion.

It is not straightforward to compare the systems based on the decomposition at the transition state, since each transition state has a different O-H distance (see Table S2). For example, the orbital interaction is almost linearly dependent on the O-H distance: the shorter this distance (towards ^{3}**2**), the greater the orbital attraction. Similarly, the strain becomes dominated by the methane strain after C-H $\sim 1.2 \div 1.3$ Å. The different O-H bondlengths are achieved when the electron donor orbital (EDO) attempts to interact with the electron acceptor orbital EAO in an optimal manner that will increase the overlap. It can be seen from Table S2 that at the transition state the overlap is in all cases practically the same.

Therefore it might be more useful to analyse the energy components at equal O-H and C-H distances. To render the detailed analysis of the energy contributions tractable we consider model transition states at which the O-H and C-H bondlengths are fixed at 1.2 and 1.3 Å respectively. Furthermore, to isolate the effect of the orbital destabilization we constrain the substrate to approach axially along the Fe-O bond of the oxidant. Thereby we only consider the $\sigma-$channel of the reaction. We first optimize the reactant complex with the constraint $\angle FeOH = \angle OHC = 180^o$. Then we optimize the intermediate (near-transition state) structure with OH=1.2 Å, CH=1.3 Å and $\angle FeOH = \angle OHC = 180°$. The so obtained reactant complex and "transition state" structures are dubbed RC' and TS', correspondingly. The main geometric parameters and energy components are

given in Table S2. The FMOs of the oxidants **1** and **2** and methane in the RC' and TS' complexes are listed in Table S1.

From Table S1 it is seen that the EAOs are all $\sigma^*(\alpha)$ and their energy differences with the methane HOMO at the TS' are ordered in the sequence $\Delta\varepsilon(^5\mathbf{1}) < \Delta\varepsilon(^3\mathbf{1}) \gtrsim \Delta\varepsilon(^5\mathbf{2}) < \Delta\varepsilon(^3\mathbf{2})$. Since at the TS' the overlaps are similar one should expect the intermediate energy barriers $E(TS') - E(RC')$ to order correspondingly,[5] unless the steric effects are different. However, the Pauli repulsion should be similar in the quintet and triplet states, because we chose an axial approach in all cases. This is indeed so, as seen from Table S2. In contrast to the relaxed transition state (TS), in the axially constrained TS' the Pauli repulsion components differ much less (within 5.9 kcal/mol). Also the electrostatic and strain contributions are comparable (within 3.8 and 3.0 kcal/mol, respectively). It is readily seen that the main contribution to the energy difference is the orbital energy. This component reflects the donor-acceptor bond strength and repeats the order of the EAO/EDO energy differences. The model, thus, qualitatively shows a relation between the acceptor-donor energy differences, the orbital interaction and the total energy barrier.

At the TS' geometry the MO energy difference $\varepsilon_{S=1}(\sigma^*(\alpha)) - \varepsilon_{S=2}(\sigma^*(\alpha))$ is 1.2 and 1.0 eV in **1** and **2**, respectively. The ligand alternation has a similar effect: $\varepsilon_{\mathbf{1}}(\sigma^*(\alpha)) - \varepsilon_{\mathbf{2}}(\sigma^*(\alpha))$ is 1.2 and 1.0 eV and $\varepsilon_{\mathbf{1}}(\pi^*(\alpha)) - \varepsilon_{\mathbf{2}}(\pi^*(\alpha))$ is 1.1 and 1.4 eV for S=2 and S=1 states, correspondingly.

Importantly, the considered model demonstrates the effect of the ligand field and spin state on the energy barrier in terms of the relative acceptor-donor orbital energy.
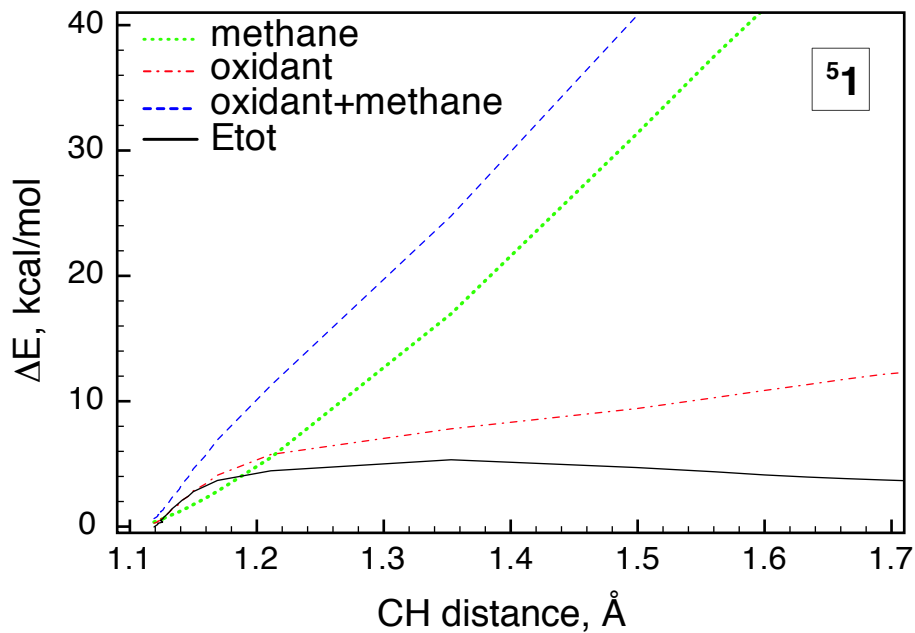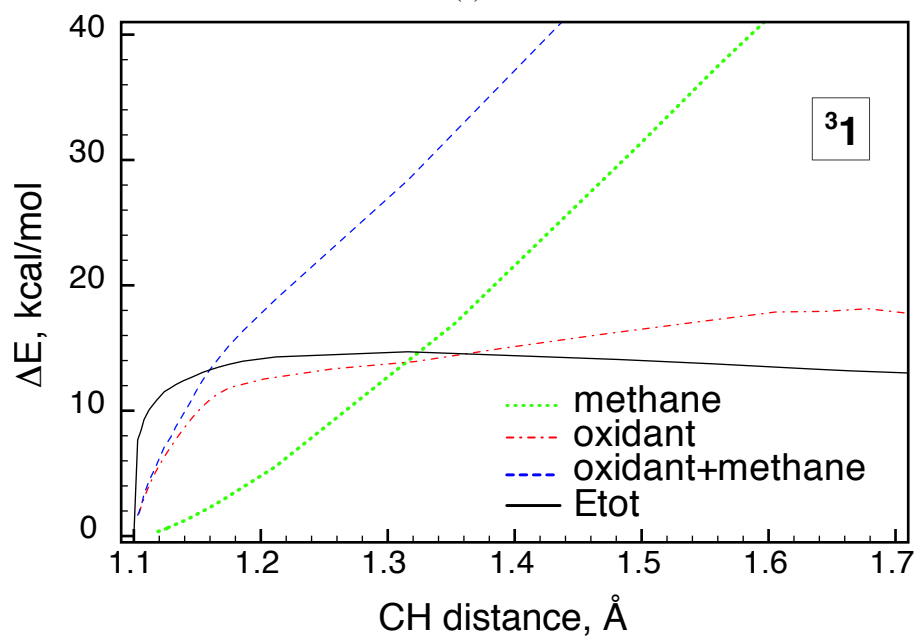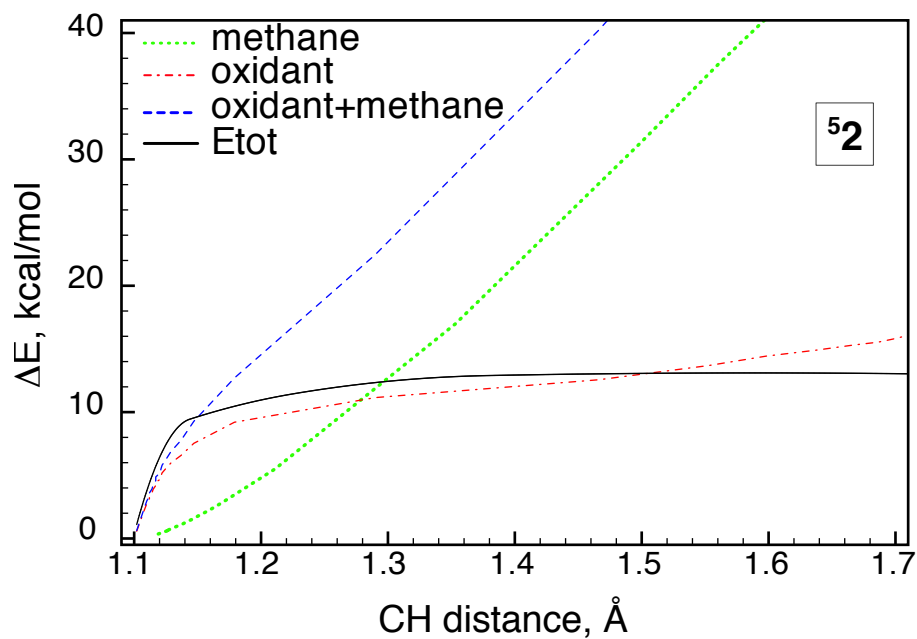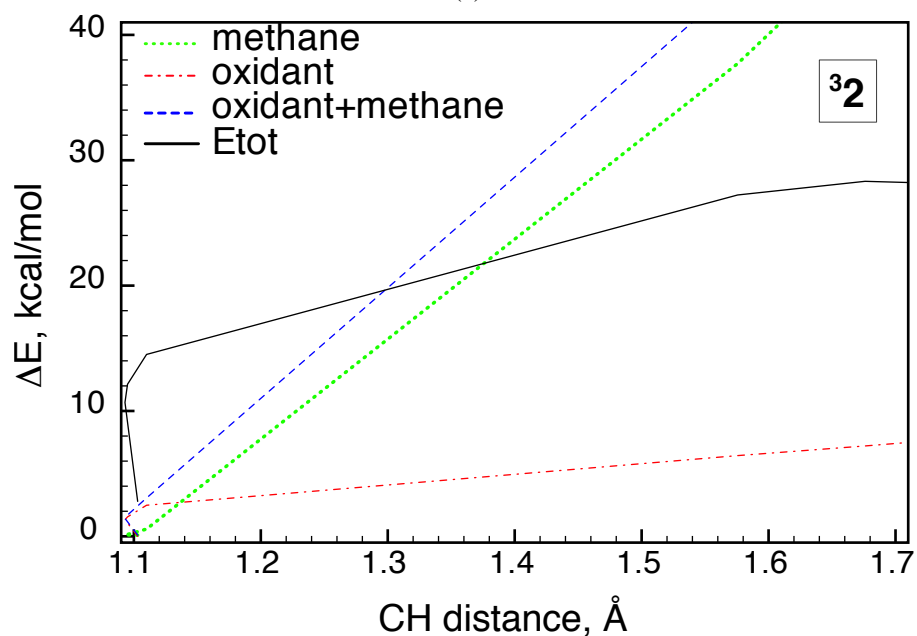
Figure S1: Strain energy contribution from the substrate (methane), and the oxidant $[FeO(H_2O)_5]^{2+}$ (**1**) in quintet (a) and triplet (b) states. The total potential energy that includes the electronic contribution (steric repulsion and orbital attraction) is given with the black solid line. The shown results have been obtained along the intrinsic reaction coordinate and projected on the C-H distance.

(a)

(b)

Figure S2: Strain energy contribution from the substrate (methane), and the oxidant $[FeO(H_2O)(NH_3)_4]^{2+}$ (**2**) in quintet (a) and triplet (b) states. The total potential energy that includes the electronic contribution (steric repulsion and orbital attraction) is given with the black solid line. The shown results have been obtained along the intrinsic reaction coordinate and projected on the C-H distance.

Table S1: Energies of the frontier MOs of the oxidants $^3\mathbf{1}$, $^5\mathbf{1}$, $^3\mathbf{2}$, and $^5\mathbf{2}$ and methane HOMO at the respective complex geometries, in eV. The energy difference $\Delta\varepsilon$ and overlap $S_{EAO,EDO}$ between the electron acceptor orbital (EAO) and donor orbital (EDO). The EAO energies are shown with boldface. The occupied and empty orbitals are labeled respectively "o" and "e".

Reactant Complex Geometry

Cpd.	S	$2\sigma\uparrow$	$\pi\uparrow$	$d_{xy}\uparrow$	$d_{x^2-y^2}\uparrow$	$\pi^*\uparrow$	$3\sigma^*\uparrow$	$2\sigma\downarrow$	$\pi\downarrow$	$d_{xy}\downarrow$	$\pi^*\downarrow$	$3\sigma^*\downarrow$	Me	$\Delta\varepsilon$	$S_{EAO,EDO}$
1	2	-18.6 o	-19.3 o	-18.8 o	-16.0 o	-15.7 o	**-13.8 e**	-18.1 o	-16.6 o	-14.5 e	-13.4 e	-12.4 e	-14.6	0.7	0.047
	1	-18.2 o	-18.6 o	-15.7 o	-13.8 e	**-15.0 o**	-12.6 e	-17.7 o	-16.4 o	-15.1 o	-13.2 e	-12.1 e	-15.7	0.7	0.026
2	2	-17.4 o	-17.8 o	-16.7 o	-18.1 o	-14.4 o	**-12.3 e**	-16.9 o	-15.6 o	-13.3 e	-12.1 e	-11.0 e	-13.8	1.5	0.033
	1	-17.0 o	-16.7 o	-14.3 o	-11.8 e	-13.6 o	-11.2 e	-16.5 o	-15.2 o	-13.7 o	**-11.8 e**	-10.6 e	-14.4	2.7	0.018

Transition State Geometry

Cpd.	S	$2\sigma\uparrow$	$\pi\uparrow$	$d_{xy}\uparrow$	$d_{x^2-y^2}\uparrow$	$\pi^*\uparrow$	$3\sigma^*\uparrow$	$2\sigma\downarrow$	$\pi\downarrow$	$d_{xy}\downarrow$	$\pi^*\downarrow$	$3\sigma^*\downarrow$	Me	$\Delta\varepsilon$	$S_{EAO,EDO}$
1	2	-18.4 o	-18.9 o	-18.7 o	-18.3 o	-15.9 o	**-14.4 e**	-18.0 o	-16.3 o	-14.5 e	-13.7 e	-13.0 e	-15.2	0.8	0.12
	1	-18.3 o	-18.7 o	-16.3 o	-14.8 e	**-15.4 o**	-13.3 e	-17.8 o	-16.4 o	-15.8 o	-13.6 e	-12.8 e	-15.9	0.4	0.10
2	2	-17.4 o	-17.6 o	-17.0 o	-18.3 o	-14.8 o	**-13.4 e**	-17.0 o	-15.5 o	-13.4 e	-12.6 e	-12.0 e	-14.5	1.0	0.13
	1	-16.6 o	-16.2 o	-16.4 o	-11.8 e	-14.0 o	-11.6 e	-16.1 o	-14.8 o	-13.7 o	**-12.3 e**	-11.1 e	-13.7	1.4	0.13

Constrained linear approach reactant complex (RC') geometry

Cpd.	S	$2\sigma\uparrow$	$\pi\uparrow$	$d_{xy}\uparrow$	$d_{x^2-y^2}\uparrow$	$\pi^*\uparrow$	$3\sigma^*\uparrow$	$2\sigma\downarrow$	$\pi\downarrow$	$d_{xy}\downarrow$	$\pi^*\downarrow$	$3\sigma^*\downarrow$	Me	$\Delta\varepsilon$	$S_{EAO,EDO}$
1	2	-18.5 o	-19.1 o	-18.6 o	-16.0 o	-15.7 o	**-13.8 e**	-18.0 o	-16.5 o	-14.4 e	-13.3 e	-12.4 e	-14.6	0.8	0.045
	1	-18.3 o	-18.5 o	-15.7 o	-13.9 e	-15.0 o	**-12.6 e**	-17.7 o	-16.3 o	-15.1 o	-13.2 e	-12.1 e	-13.9	1.3	0.022
2	2	-17.4 o	-17.8 o	-16.8 o	-18.1 o	-14.4 o	**-12.4 e**	-16.9 o	-15.6 o	-13.3 e	-12.1 e	-11.0 e	-13.9	1.6	0.001
	1	-17.0 o	-16.7 o	-14.4 o	-11.8 e	-13.6 o	**-11.2 e**	-16.5 o	-15.3 o	-13.7 o	-11.8 e	-10.6 e	-13.5	2.3	0.015

Constrained linear approach near-transition state (TS') geometry

Cpd.	S	$2\sigma\uparrow$	$\pi\uparrow$	$d_{xy}\uparrow$	$d_{x^2-y^2}\uparrow$	$\pi^*\uparrow$	$3\sigma^*\uparrow$	$2\sigma\downarrow$	$\pi\downarrow$	$d_{xy}\downarrow$	$\pi^*\downarrow$	$3\sigma^*\downarrow$	Me	$\Delta\varepsilon$	$S_{EAO,EDO}$
1	2	-18.4 o	-18.9 o	-18.7 o	-16.3 o	-15.9 o	**-14.4 e**	-18.0 o	-16.4 o	-14.5 e	-13.6 e	-12.9 e	-15.4	1.0	0.12
	1	-18.1 o	-18.3 o	-16.0 o	-14.3 e	-15.3 o	**-13.2 e**	-17.7 o	-16.2 o	-15.4 o	-13.5 e	-12.7 e	-15.2	2.0	0.12
2	2	-17.5 o	-17.6 o	-16.9 o	-18.3 o	-14.8 o	**-13.2 e**	-17.0 o	-15.6 o	-13.4 e	-12.5 e	-11.9 e	-14.9	1.7	0.12
	1	-17.1 o	-16.8 o	-14.5 o	-12.0 e	-13.9 o	**-12.2 e**	-16.6 o	-15.3 o	-13.9 o	-12.1 e	-11.6 e	-14.5	2.3	0.12

Table S2: Key geometric parameters and energy decomposition of the complexes $1+CH_4$ and $2+CH_4$ in the quintet (S=2) and triplet (S=1) states in the reactant complex (RC) and transition state (TS). At the constrained reactant RC' and transition state TS' complexes the substrate is allowed to approach linearly along the Fe-O axis. Bondlengths are in Å and angles in degrees. Energy decompositions at the TS and TS' are relative to the respective reactant complexes RC and RC', in kcal/mol. The relative total bonding energy is decomposed as $\Delta E = \Delta E_{Tot}^{Strain} + \Delta E^{Pauli} + \Delta E^{Elstat} + \Delta E^{Orb}$, where ΔE_{Tot}^{Strain} is the total of the oxidant and methane strain, ΔE^{Pauli}, ΔE^{Elstat} and ΔE^{Orb} are the Pauli repulsion, electrostatic and the orbital attraction contributions, respectively.

Completely relaxed structures

| | | Geometric parameters | | | | | Energy decomposition at TS | | | | | |
| | | RC | | TS | | | | | | | | |
Cpd.	S	O-H/C-H	$\gamma_{FeOH}/\zeta_{OHC}$	O-H/C-H	$\gamma_{FeOH}/\zeta_{OHC}$	ω, i cm^{-1}	ΔE_R^{Strain}	ΔE_{Tot}^{Strain}	ΔE^{Pauli}	ΔE^{Elstat}	ΔE^{Orb}	ΔE
1	2	2.10/1.12	177/172	1.21/1.35	165/177	824	7.8	24.8	117.5	-37.0	-99.7	5.5
	1	2.95/1.10	107/154	1.26/1.32	128/171	695	14.6	28.4	101.1	-32.8	-81.6	15.1
2	2	2.39/1.10	176/176	1.12/1.47	165/179	409	12.6	40.2	156.1	-49.7	-134.1	12.6
	1	3.52/1.10	121/122	1.09/1.58	128/167	607	6.4	44.2	180.5	-63.8	-133.6	27.3

Constrained linear approach structures

| | | Geometric parameters | | | | Energy decomposition at TS' | | | | | |
| | | RC' | | TS' | | | | | | | |
Cpd.	S	O-H/C-H	$\gamma_{FeOH}/\zeta_{OHC}$	O-H/C-H	$\gamma_{FeOH}/\zeta_{OHC}$	ΔE_R^{Strain}	ΔE_{Tot}^{Strain}	ΔE^{Pauli}	ΔE^{Elstat}	ΔE^{Orb}	ΔE
1	2	2.04/1.12	180/180	1.20/1.30	180/180	6.7	18.6	117.5	-35.8	-94.8	5.4
	1	2.52/1.10	180/180	1.20/1.30	180/180	5.3	17.1	123.4	-38.4	-85.4	16.7
2	2	2.44/1.09	180/180	1.20/1.30	180/180	8.4	20.1	122.1	-38.4	-92.0	11.8
	1	2.76/1.10	180/180	1.20/1.30	180/180	7.2	18.2	122.4	-39.0	-79.5	22.1

References

(1) Bickelhaupt, F. M.; Baerends, E. J. *Rev. Comp. Chem.* **2000**, *15*, 1–86.

(2) ADF 2010.01, SCM, Theoretical Chemistry, Vrije Universiteit Amsterdam, The Netherlands;. 2010; `http://www.scm.com`.

(3) Baerends, E.; Ellis, D.; Ros, P. *Chem. Phys.* **1973**, *2*, 41–51.

(4) Fonseca Guerra, C.; Snijders, J.; Te Velde, G.; Baerends, E. *Theor. Chem. Acc.* **1998**, *99*, 391–403.

(5) Louwerse, M. J.; Baerends, E. J. *Phys. Chem. Chem. Phys.* **2007**, *9*, 156–66.